Title

Mass balance implies Holocene development of a low-relief karst patterned landscape

Authors

Chamberlin, Catherine A
Bianchi, Thomas S
Brown, Amy L
et al.

Publication Date

2019-11-01

DOI

10.1016/j.chemgeo.2018.05.029

Peer reviewed

Chemical Geology xxx (xxxx) xxx–xxx

Contents lists available at ScienceDirect

Chemical Geology

journal homepage: www.elsevier.com/locate/chemgeo

Mass balance implies Holocene development of a low-relief karst patterned landscape

Catherine A. Chamberlin[a,*], Thomas S. Bianchi[b], Amy L. Brown[b], Matthew J. Cohen[c], Xiaoli Dong[a], Madison K. Flint[b], Jonathan B. Martin[b], Daniel L. McLaughlin[d], A. Brad Murray[a], Andrea Pain[b], Carlos J. Quintero[e], Nicholas D. Ward[b,1], Xiaowen Zhang[b], James B. Heffernan[a]

[a] Nicholas School of the Environment, Duke University, Environment Hall, 9 Circuit Drive, Box 90328, Durham, NC 27708, United States
[b] Department of Geological Sciences, University of Florida, 241 Williamson Hall, PO Box 112120, Gainesville, FL 32611, United States
[c] School of Forest Resources and Conservation, University of Florida, 136 Newins-Ziegler Hall, PO Box 110410, Gainesville, FL 32611, United States
[d] The Department of Forest Resources and Environmental Conservation, Virginia Polytechnic Institute and State University, Cheatham Hall, 310 W Campus Dr, Blacksburg, VA 24061, United States
[e] The Department of Soil and Water Sciences, University of Florida, 1692 McCarty Dr, Gainesville, FL 32603, United States

ARTICLE INFO

Editor: Michael E. B

Keywords:
Biokarst
Mass balance
Chemical denudation
Self-organization
Calcium
Phosphorus
Weathering

ABSTRACT

We constructed mass balances of both calcium and phosphorus for two watersheds in Big Cypress National Preserve in southwest Florida (USA) to evaluate the time scales over which its striking landscape pattern developed. This low-relief carbonate landscape is dotted with evenly spaced, evenly sized, shallow surface depressions that annually fill with surface water and thus support wetland ecosystems (e.g. cypress domes) embedded in a pine-dominated upland matrix with exposed bedrock. Local and landscape scale feedbacks between hydrology, ecological dynamics and limestone dissolution are hypothesized to explain this karst dissolution patterning. This hypothesis requires the region to be wet enough to initiate surface water storage, which constrains landscape formation to interglacial periods. The time scale therefore would be relatively recent if creation of the observed pattern occurred in the current interglacial period (i.e. Holocene), and older time scales could reflect inherited patterns from previous inter-glacial periods, or from other processes of abiotic karstification. We determined phosphorus stocks across four landscape compartments and estimated the limestone void space (i.e., wetland depression volume) across the landscape to represent cumulative calcium export. We calculated fluxes in (e.g., atmospheric deposition) and out (i.e., solute export) of the landscape to determine landscape denudation rates through mass balance. Comparing stocks and annual fluxes yielded independent estimates of landscape age from the calcium and phosphorus budgets. Our mass balance results indicate that the landscape began to develop in the early-mid Holocene (12,000–5000 ybp). Radiocarbon dating estimates implied similar rates of dissolution (~1 m per 3000–3500 years), and were in agreement with Holocene origin. This supports the hypothesis that ecohydrologic feedbacks between hydrology and vegetation occurring during the present interglacial period are sufficient to shape this landscape into the patterns we see today, and more broadly suggests the potential importance of biota in the development of macro-scale karst features.

1. Introduction

Karst landscapes, due to the highly soluble nature of their rock, export their weathering products hydrologically, creating a wide variety of features such as caves, karst towers, and dissolution holes, but also causing natural hazards such as sink holes (Ford and Williams, 2007). Preferential flow paths through the landscape attract disproportionately large volumes of water, and this water, which is undersaturated with respect to carbonate, dissolves the rock along the conduit walls and creates a positive feedback loop of dissolution and flow (Akiyama et al., 2015; Perne et al., 2014; Sweeting, 1973). These conduits are classically subsurface (e.g. cave formation) but in the right

Abbreviations: RP, Raccoon Point; TR, Turner River; BICY, Big Cypress National Preserve; TIC, Total Inorganic Carbon

* Corresponding author.
E-mail addresses: catherine.chamberlin@duke.edu (C.A. Chamberlin), tbianchi@ufl.edu (T.S. Bianchi), amy.brown@ufl.edu (A.L. Brown), mjc@ufl.edu (M.J. Cohen), xiaoli.dong@duke.edu (X. Dong), mflint@ufl.edu (M.K. Flint), jbmartin@ufl.edu (J.B. Martin), mclaugd@vt.edu (D.L. McLaughlin), abmurray@duke.edu (A.B. Murray), ajpain@ufl.edu (A. Pain), carlosjquintero@ufl.edu (C.J. Quintero), nicholas.ward@pnnl.gov (N.D. Ward), xz510@ufl.edu (X. Zhang), james.heffernan@duke.edu (J.B. Heffernan).
[1] Present Address: Marine Sciences Laboratory, Pacific Northwest National Laboratory, 1529 W Sequim Bay Rd, Sequim, WA 98382, United States.

https://doi.org/10.1016/j.chemgeo.2018.05.029
Received 28 August 2017; Received in revised form 16 March 2018; Accepted 21 May 2018

circumstances can also be surface drainage (e.g. sections of fluviokarst). Karst systems are distinct from siliciclastic systems in that their morphology is governed more by dissolution than by mechanical erosion, though often both processes occur (Covington et al., 2015; Dubois et al., 2014; Ryb et al., 2014).

The solubility of carbonate rocks depends on the pH of the water contacting it (Plummer and Wigley, 1976; Plummer et al., 1978; Sweeting, 1973). Though rainwater has moderate acidity due to dissolved carbonic acid in equilibrium with atmospheric CO_2 (Martin, 2017), biological respiration can greatly intensify acidity of soil and vadose zone water (Folk et al., 1973; Liu et al., 2007; Yang et al., 2015). Many studies have shown that dissolution of karst bedrock is highly dependent on soil pCO_2, which is a by-product of biological activities such as heterotrophic and root respiration (Calmels et al., 2014; Hu and Burdige, 2007; Khadka et al., 2014; Solomon and Cerling, 1987; Zhao et al., 2010). Biological processes can also promote calcium carbonate deposition through transpiration or CO_2 removal from solution by aquatic photosynthesis (de Montety et al., 2011; Hu and Burdige, 2007; Sullivan et al., 2016). Disturbances and changes of biota can therefore have direct impacts on karst landscape formation (e.g. Coleborn et al., 2016).

The term biokarst has been coined to describe landscapes in which biological processes drive karstification, creating features on a range of scales (de la Rosa, 2016; Duane et al., 2003; Fiol et al., 1996; Viles, 1984). In one extreme, all karst may be considered biologically linked, as the evolution of photosynthetic life produced the carbonate rock necessary for karst formation, fundamentally linking the two processes in evolutionary time (Phillips, 2016a). However, biokarst generally refers to more recent feedbacks, such as heterogeneity in organic matter cycling (via primary production and respiration) or mechanical activities of plants or animals, which dramatically accelerate local weathering. Biokarsts in some cases have been known to develop since the last glaciation (i.e. during the Holocene), reflecting the potential rapidity of this form of landform development (de la Rosa, 2016), but the timescales over which biokarst features develop remain largely unresolved. Connecting weathering rates to the geometry and developmental timescales of karst features is essential to understanding the development of these landscapes, however few studies have explicitly linked rates of weathering with the time- and length-scales of karst landforms (see Florea, 2015), and none have done so for large, regular features such as those found in Big Cypress.

In the karst landscape of Big Cypress National Preserve (BICY) in south Florida, regularly-patterned depressional wetlands support greater primary productivity, hydric soil conditions, and consequent accretion of organic matter (Cohen et al., 2011). The regular size and spacing of these depressions suggests self-organization (Camazine, 2001; Rietkerk and van de Koppel, 2008), leading to the hypothesis that BICY is a biokarst landscape in which biota shape the limestone through local positive feedbacks among hydrology, wetland processes (productivity and respiration), and dissolution, and negative feedbacks on these processes at a landscape scale, e.g. through water limitation (Cohen et al., 2011; Watts et al., 2014). Cypress trees, the dominant wetland species in the depressions, colonized the area only at the beginning of the Holocene when sea level rose and the region became wetter (Watts, 1975; Watts and Hansen, 1994), allowing surface inundation and support of wetland ecosystems (Thornberry-Ehrlich, 2008; Toscano and Macintyre, 2003). Consequently, it is hypothesized that biokarst development by biota is relatively recent, with initiation constrained to the early Holocene. Plausible alternative hypotheses, that depressions are either collapse features (e.g. collapse sinkholes) or inherited features reflecting older land-forming processes (even potentially the same ecohydrologic feedbacks, but over multiple interglacial periods), would not predict correspondence between landscape-scale weathering rates, the volume of depressions, and the onset of modern hydrology and biotic assemblages. Here, we test this prediction of recent origin.

To test this prediction, we constructed elemental budgets for both calcium (Ca) and phosphorus (P) to estimate rates of contemporary weathering and patterned landscape age across the BICY landscape. We determined inputs, storage, and export of Ca (the primary mineral constituent of bedrock) and P (an essential and likely limiting element for biological growth), and estimated landscape age from these budgets based on measured void volumes and P accumulation, both jointly and independently. We confront these mass-balance derived age estimates with radiocarbon dates, paleoclimatic records, and weathering rates derived from a mechanistic reaction-transport model, each of which is linked to the conditions and processes that we hypothesize created the distinct Big Cypress landscape.

2. Methods

2.1. Study site

Big Cypress National Preserve is a low-relief karst landscape in southern Florida west of the Everglades. The gain in elevation is 0.03–0.15 m km^{-1}, and the whole landscape rests on the Late Miocene to Pliocene Tamiami formation - a 45 m deep formation of limestone cobbles mixed with sandstone, mud and clay (Mcpherson, 1974; Thornberry-Ehrlich, 2008). Underlying the Tamiami formation is the Hawthorn Group, a thick Miocene aquiclude primarily composed of clay (Mcpherson, 1974). Hydrologically, BICY receives water primarily from rainwater, and though parts of BICY drain into the Everglades, no surface water flows into BICY (Mcpherson, 1974; Shoemaker et al., 2011). The region has a humid subtropical climate with an average annual precipitation of 1330 mm (Mcpherson, 1974). Rainfall is spread across distinct dry (Oct–Apr) and wet (Apr–Oct) seasons (Shoemaker et al., 2011). As such, landscape export of water and solutes is highly seasonal, with marked switches between high and low discharge in response to critical surface connectivity thresholds (McLaughlin D.L. 2017, personal communication).

The landscape is characterized by regularly spaced depressions in the surface-exposed limestone bedrock. Sediments in the depressions are markedly deeper (up to 300 cm) than in the uplands (5–10 cm) and also contain far higher organic matter content (Watts et al., 2014). These depressions support numerous wetland species but are typically dominated by cypress trees, which grow taller in the center of the depressions than on the circumference, creating a domed shape (Fig. 1). Previous work has indicated that the variation in height is due to a difference in growth rate rather than age (Ewel and Wickenheiser, 1988), though disturbances such as wildfire and extended periods of dry soil in the uplands may reinforce this structure (Monk and Brown, 1965; Watts et al., 2012). Variations in cypress heights from the wetland center to edge leads to the name cypress domes, though the shape of the surface sediments and bedrock is actually a depression, with a drop in surface elevation of up to 1.5 m between the upland and the wetland center accompanied by a more dramatic difference in bedrock elevation of up to 3 m (Watts et al., 2014). Flooding duration varies with surface elevation throughout the landscape, with many depressions inundated for the entire year while the surrounding uplands may never be inundated (Cohen et al., 2011).

Pond Cypress (*Taxodium ascendens*) is typically the dominant species in depressional wetlands with smaller populations occurring of southern wax myrtle (*Myrica cerifera*), alligator apple (*Annona glabra*), cocoplum (*Chrysobalanus icaco*), and coastal plain willow (*Salix caroliniana*). In parts of the landscape, large wetland depressions lack trees in the center, and some are entirely devoid of cypress trees and instead are dominated by willow and sawgrass (*Cladium jamaicense*). Vegetation of the surrounding uplands varies with elevation and associated hydrologic regime and is dominated by palmetto (*Sabal palmetto*) and slash pine (*Pinus elliottii*) in drier regions and by dwarf cypress and wet prairies of hairawn muhly (*Muhlenbergia capillaris*) in wetter areas. Wildfire is common in the landscape and likely maintains the

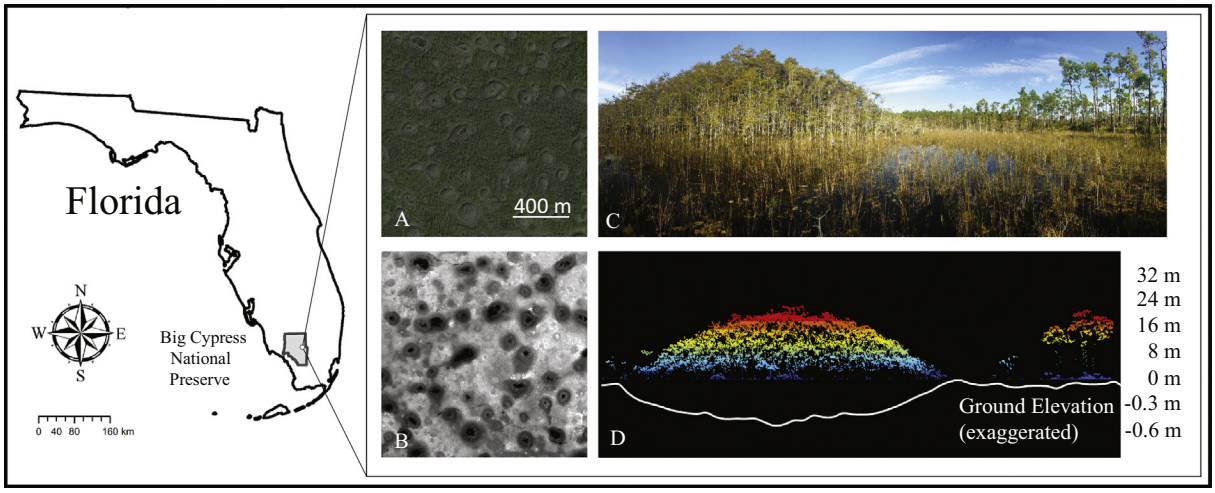

Fig. 1. Aerial and ground-level images of BICY.
A) Satellite image of a domain in RP; Imagery © 2017 Google. B) LiDAR high resolution DEM of the same domain. C) Panorama view of an intensively sampled dome and the surrounding pine matrix in RP. D) The LiDAR point cloud results of the same dome. LiDAR data provided by the National Center for Airborne Laser Mapping.

patchiness of the landscape in a dynamic equilibrium (Cohen et al., 2011; Watts et al., 2012).

Big Cypress has been minimally impacted by humans compared to the neighboring Everglades. However, logging in the past century, farming in some areas before 1940, oil drilling and recreation have led to the construction of elevated roadways which restrict free flow of water across the landscape and constrict connectivity of the divided landscape to small culverts evenly spaced underneath the roadways. Road construction has been accompanied by canal construction since the 1920s, and the landscape now drains primarily through canals dug along natural flow paths (Mcpherson, 1974).

The climate and vegetation of South Florida have changed distinctively between the Pleistocene and Holocene. Towards the end of the Pleistocene, sea levels were ~30 m lower and the landmass of Florida much wider. Sea level rise appears to have been non-linear with a sharp transgression and regression that would have inundated only the most southern parts of the preserve (Mitchell-Tapping et al., 1996; Parkinson, 1989; Toscano and Macintyre, 2003). Climate in the region shifted from a more arid to a more humid climate, with many lakes in the region forming ~8000 years ago (Watts, 1975). This was accompanied by the shift from a shrub-oak dominated system to modern vegetation. Pollen studies to the north of BICY show transitions from oak dominant assemblages to pine and cypress assemblages around 5000–10,000 years ago (Watts, 1975; Watts and Hansen, 1994). Thus, interactions between hydrologic regimes and wetland processes that are hypothesized to cause the development of depressions are likely to have established early in the Holocene, approximately 10,000 years ago.

2.2. Mass balances for landscape age

2.2.1. Construction of mass balance

We estimated landscape ages using mass balances for both Ca and P. Budget construction requires accurate accounting of elemental fluxes both into and out of a system, as well as estimates of all storage compartments within a system. Here, we construct budgets for systems defined horizontally by watershed boundaries (see Section 2.3) and vertically at the soil-bedrock interface. As dissolution of bedrock causes this interface to move deeper over time, we allowed the vertical boundary of our system to shift as well. Our approach assumes that the landscape was initially flat, and that negligible stores of P were found initially in sediments and vegetation. The first assumption is likely valid because of the very low slope of the landscape and because of its location on the coastal plain. The second was initially made as a simplifying assumption, but is validated by the minimal pools of P in modern upland soils, and substantial P accumulation in the soils of the depressions.

Chemical fluxes for our system boundaries consist of annual atmospheric deposition, dissolved export (i.e., mass flux out of a watershed), and dissolution inputs from the underlying bedrock (Fig. 2). Deposition and export were both estimated from published data (see Sections 2.4.1 and 2.4.2), whereas dissolution inputs were derived using mass balances (Fig. 2). Phosphorus storage compartments within the system boundaries included soil, vegetation, standing water, and periphyton, whereas calcium storage compartments only included the water and the soil because calcium is found in very low concentrations in most organisms (Sterner and Elser, 2002).

2.2.2. Age calculations

Using this mass balance approach, we calculated landscape generation age using three methods (Fig. 2), all of which assume that modern measured fluxes are representative of those occurring during the relative climatic and ecological stability of the Holocene. In the first, we used the ratio of void volume to Ca export as an estimate of age, for the second, we used the accumulation rate of P, and for the third we used the accumulation rates of P and Ca together. We applied each of these calculations separately for two delineated watersheds in BICY and to the aggregated landscape. The first calculation (Calcium method) used the calcium budget to yield a dissolution rate (g yr^{-1}) by assuming no net change in soil Ca storage over time. Assuming then that all Ca dissolution occurred in depressions, we were able to use the depression volumes (see Section 2.5) as estimates of cumulative Ca loss and derived an age estimate as described in Fig. 2a. Though dissolution more likely occurs throughout the landscape, the majority of dissolution likely occurs in the depressions because of the longer hydroperiods and because of increased biological respiration, and thus the void space would account for the bulk of lost Ca. This assumption of where dissolution occurs is able to be relaxed in our third method in which we allow for non-zero change in storage. The second calculation (Phosphorus method) used the Ca budget-derived dissolution rate (adjusted using the Ca/P ratio of the bedrock) to determine the age necessary to accumulate observed P stocks with observed net P fluxes (Fig. 2b). The third approach (Joint method) assumed that the age of the landscape according to the Ca and P budgets were identical and could therefore be solved jointly (Fig. 2c). This allowed us to include accumulated calcium stocks on the landscape (e.g. in sediments) and solve for the dissolution rate as a second dependent variable alongside the age of the system instead of directly inferring it from the calcium mass flux out of the system. Doing so also allowed us to relax assumptions about where

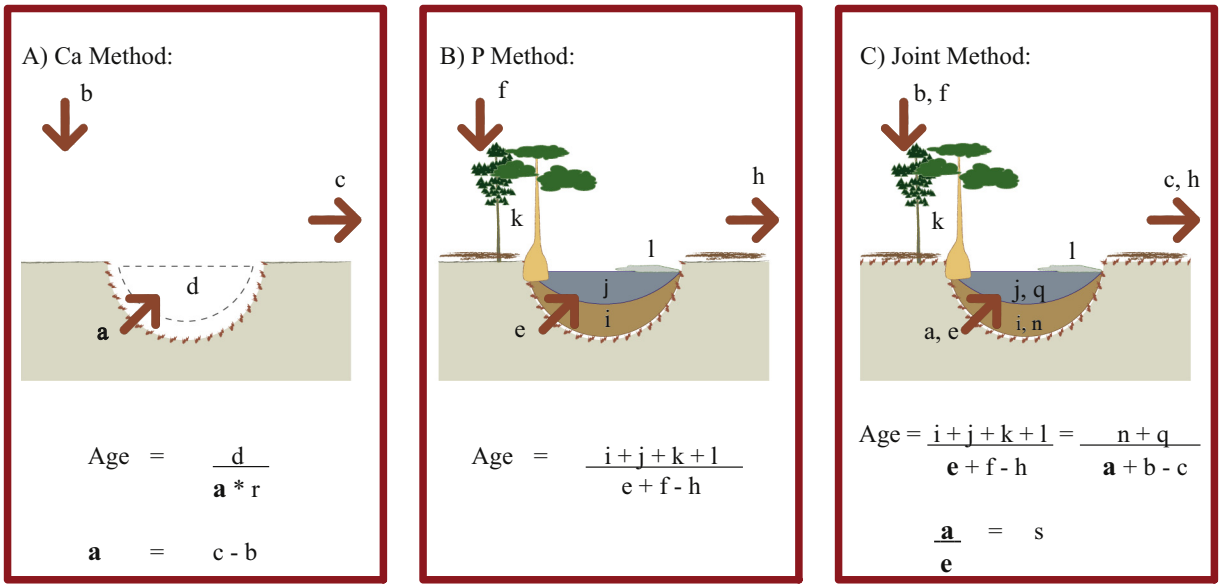

Fig. 2. Schematic of mass balance elements used for age calculations.
A depiction of the parts of the mass balance used for A) the Ca method, B) the P method, and C) the Joint method. Red dotted boundaries are where dissolution and/or precipitation is allowed to occur in each method. In A and B, dissolution occurs only in the depressions and that mass dissolution rate represents landscape denudation. The dissolution inputs in B are defined as the dissolution input in A multiplied by the stoichiometric P/Ca ratio of the rock. In C the uplands are allowed to either dissolve or grow (via precipitation), which causes the mass dissolution rate in the depression to differ from the landscape denudation rate. Equations show how age was estimated, and bolded variables are unknowns. *a*, *b* and *c* are the rates of Ca input by dissolution, deposition, and export, respectively (g yr^{-1}). *d* is the void volume (m^3). *e*, *f*, and *h* are the rates of P input by dissolution, deposition, and export, respectively (g yr^{-1}). *e* is defined in the P method but solved for as an unknown in the Joint method. *i*, *j*, *k* and *l* are the amounts of P stored in the soil, water, vegetation and periphyton, respectively (g), and *n* and *q* are the amounts of Ca stored in the soil and water (g). *r* is the calcium content of the caprock (g m^{-3}) and *s* is the Ca/P ratio of the caprock. We assumed the caprock was representative of the bedrock. (For interpretation of the references to colour in this figure legend, the reader is referred to the web version of this article.)

denudation occurred or what the total volume lost is, and thus allowed the potential for redistribution of dissolved bedrock and dissolution in the uplands (Fig. 2).

As an empirical independent check on the mass balance analysis we also radiocarbon dated charcoal found at depths in the depressions (Section 2.7.3).

2.2.3. Monte Carlo approach

We did all calculations 10,000 times in a Monte Carlo simulation. This allowed us to propagate uncertainty from our many budget variables easily through the steps necessary to calculate the age. Each input to the calculations was represented as a distribution, and by randomly combining inputs sampled from these distributions, we were able to quantify the uncertainty associated with our results. All computations were done using R statistical software version 3.3.3.

2.3. Watershed estimation and water fluxes

For our mass balance, we needed to define the boundaries of the ecosystem. We wanted to bind the system horizontally by the edges of the watershed so that the chemical and hydrologic fluxes would be coupled (Bormann and Likens, 1967). Due to the very flat nature of BICY, the traditional method of delineating catchments based on topography was untenable, even with high-resolution LiDAR digital elevation models. Instead, we used a closed water balance to calculate the size of the watersheds. To construct this water balance we needed to know the volume of water flowing out of the watershed each year ($m^3\,yr^{-1}$), and the available water each year (m yr^{-1}) which was the difference between precipitation (m yr^{-1}) and ET (m yr^{-1}).

Several roads with culverts and canals run north-south dividing the preserve, and so we assumed that water on the eastern section (Raccoon Point - RP) would ultimately be intercepted and drain through the canal network on that side to a common drainage canal, and water on the western section (Turner River - TR) would ultimately drain through a canal draining a canal network on that side. Since these sides of the landscape would not be connected by surface flow, we were able to calculate the size of two watersheds, an "RP" watershed and a "TR" watershed. Both canals draining these two sections of the landscape have daily discharge available from the USGS and South Florida Water Management District (http://www.sfwmd.gov/dbhydro) for the past ~50 years. Annual discharge rates were calculated by summing daily discharge over the entire water year beginning October 1.

Three years of published latent energy data (Shoemaker et al., 2011) were converted to actual evapotranspiration assuming $AET = L_e/(P_w * \lambda)$ where L_e is latent heat flux, P_w is the density of water, and λ is the latent heat of vaporization. As the data were partitioned by habitat type, including dwarf cypress, wet prairie, piney upland, and cypress swamp (i.e. cypress domes or wetland depressions), we determined the estimated percent cover of wetland depressions by LiDAR (Section 2.5), and used a vegetation map of the preserve (Thornberry-Ehrlich, 2008) to estimate the percent cover of the other habitats for RP and TR separately. Precipitation data accompanying the evapotranspiration calculations allowed us to calculate annual available water on a depth basis (mm yr^{-1}) for each of the 3 years and 4 habitat types (Shoemaker et al., 2011). We could then calculate the average available water of the landscape by weighting the available water for the individual habitat types by their percent coverage of the whole landscape. In the Monte Carlo simulations, available water for the habitat types were represented as a normal distribution derived from the mean and standard deviation of the 3 years of data, and percent cover of each habitat was represented as a uniform distribution of our estimated percent cover ± 5%, however it was constrained such that they always summed to 100%.

We used both annual discharge and annual available water to solve the water budget for watershed size as $Watershed\ Area\ (m^2) = \frac{Annual\ Discharge\ (m^3\ yr^{-1})}{Annual\ Available\ Water\ (m\ yr^{-1})}$. Annual discharge for each watershed in our Monte Carlo simulation was a random

sampling from the 50 year dataset. We made no attempt to correlate discharge with annual available water, as this relationship is unknown. The size of the BICY landscape was then the sum of the RP and TR watersheds, which may not be entirely consistent with the traditional delineation of the landscape via habitat assessment.

2.4. Estimations of chemical fluxes

2.4.1. Deposition

Data for annual wet deposition of Ca came from the National Atmospheric Deposition Program's data in the Everglades (http://nadp.sws.uiuc.edu/data/sites/siteDetails.aspx?net=NTN&id=FL11). We assumed total deposition to be twice that of wet deposition (an assumption warranted on a broad scale for other solutes such as chloride, see CASTNET data http://nadp.isws.illinois.edu/committees/tdep/tdepmaps/), and modeled it as a normal distribution, which the Monte Carlo simulation sampled from. Phosphorus deposition was represented by sampling a normal distribution of mean 0.036 $g\,m^{-2}\,yr^{-1}$ as reported in the literature (Ahn and James, 2001; Davis and Ogden, 1994; Redfield, 2002) and using the same coefficient of variation as the Ca deposition data.

2.4.2. Dissolved export

Both the RP and TR canals have historical chemistry records available alongside the daily discharge data (http://www.sfwmd.gov/dbhydro). We used these data to estimate annual mass flux out of the canals for the years of record. As chemical data were sparser than discharge, and the records were shorter (20–40 years), we used a log-log regression of the flow-concentration relationship to populate missing days and then aggregated them to produce annual export rates. The Monte Carlo simulation was populated with mass fluxes that corresponded to discharge in each simulation.

2.4.3. P inputs from dissolution

As described above, dissolution rates were solved as unknowns in both the Ca and Joint methods. The P method, however, used dissolution rates derived from the calcium balance, requiring conversion of those Ca mass input rates to P inputs. To determine the Ca/P ratio of the bedrock, caprock samples from the matrices surrounding two domes in RP and two domes in TR were collected in March 2016. Chemical analysis for Ca and P is described in Section 2.7.1.

2.5. Estimates of volume lost

As previously described, the Calcium method used balance-derived dissolution rates ($g\,Ca\,yr^{-1}$, Fig. 2a) to determine time required for observed cumulative Ca mass loss in the bedrock, and assumed that all dissolution occurred in depressions. We estimated cumulative mass loss as the product of cumulative depression volume and Ca content in bedrock. Using the caprock described in Section 2.4.3, we measured the bulk density volumetrically with water, and the chemical concentration as described in Section 2.7.1.

We obtained estimates of depressional area from LiDAR obtained from the National Center for Airborne Laser Mapping (NCALM) and further processed this information to delineate separate cypress wetlands (Quintero C.J., 2017, personal communication). To summarize, depression features on the landscape were delineated using the fill-difference method as outlined in Doctor and Young (2013) using aerial imagery and our knowledge of the landscape as a guide. We took the resulting map of depressional area and converted it into a binary map in which we were able to extract estimates of depressional and non depressional area on our landscape.

The depths of the depressions were calculated as the sum of the average sediment and water depths (see Sections 2.6.2 and 2.6.3 respectively). The volume was found by multiplying the depth by the depressional area in the watershed. Surface depressions were considered to represent the whole of the dissolution features in the landscape.

2.6. Estimates of storage compartments

2.6.1. Estimates of P in the vegetation compartment

To determine the size of the vegetation compartment, we undertook a vegetation survey in 6 depressional wetlands: three in RP and three in TR in October and November 2014. The upland matrices surrounding 5 of these wetlands (three in RP, two in TR) were surveyed in March 2016. Two of the RP sites were surrounded by piney upland matrices, and one was surrounded by dwarf cypress. Uplands of mixed pine and dwarf cypress surrounded both TR sites. We used the point-center-quarter method (Mitchell, 2015) to determine canopy species abundance and basal area in each of the surveyed locations.

For P biomass content, cypress and pine wood samples were collected from 5 wetland depressions and their surrounding uplands in March 2016. We selected trees at 10 meter intervals along transects laid from the center of the depressions to the middle of the surrounding upland matrices and completed one transect of 80–100 m in each wetland. We collected wood cores from the main stem at breast height in order to average across the age of the tree. We did not quantify or sample foliage on the assumption that wood accounts for most biomass. The chemical analysis of wood samples is described in Section 2.7.1.

We calculated the biomass of pine and cypress trees in the wetland depressions and in the upland matrices using the mean basal densities calculated by the point-quarter-center method and allometric equations that depended on diameter breast height (Chojnacky et al., 2014). We then converted these measurements to areal concentrations of P in vegetation using the calculated P content of wood from the chemical analysis. The areal concentrations of P were calculated separately between habitat landcover types and between TR and RP sites. As we had no samples from a wet prairie in RP, we assumed that areal P concentrations there were identical to the dwarf cypress areas in that watershed. Surveys in the matrices of the TR sites were not well distributed between these three matrix types and thus only two habitat types (depressional wetland and upland matrix) were used in TR to calculate the P vegetation compartment storage. P stored in vegetation for the whole landscape was estimated by combining the habitat specific areal concentrations with the habitat extent on the landscape in the Monte Carlo simulation.

2.6.2. Estimates of P and Ca in the sediment compartment

Sediment depth sampling locations were randomly assigned in and around the 6 intensively studied depressions from Section 2.6.1. At each sampling location a steel tile probe was driven into the ground until refusal. A meter stick was used to collect water level measurements, which were subtracted from the refusal depth to yield the sediment depth. Each of the sampling locations was also subsampled in each of the cardinal directions; North, South, East, West at respective distances of 1,3,10 and 5 m. In order to reduce the possibility of erroneous measurements, points were resampled whenever a root or other obstruction was encountered. Tile probe measurements from the surveyed features were averaged to provide average sediment depths of domes in RP and TR separately and of the upland matrices in RP and TR separately.

A minimum of three sediment cores were collected in each of these 6 depressions: at the center of the depression, mid-way between the center and the edge of the depression, and at the edge of the depression. Bulk density was measured for each core using a GeoTech Multi-sensor Core Logger. Cores were then split and sub-sampled at 5 cm increments for chemical analysis. Samples were freeze-dried, woody material > 250 μm was removed, and samples were homogenized. Chemical analysis of P and Ca content is described in Section 2.7.2.

We calculated the stocks of sediment P and Ca by partitioning our P-content, Ca-content, bulk density and sediment depth data between the

depressional wetlands and a generic "upland matrix" for RP and TR. The "upland matrix" was used because sediment sampling was done intensively in fewer locations rather than extensively across the landscape, which disallowed partitioning among the habitat types. We note that the uplands uniformly have shallow soils, with considerable area of exposed limestone suggesting generally small soil stocks.

2.6.3. Estimates of P and Ca in the water compartment

To determine the elemental stocks present in surface water, we needed to know the depth of the water on the landscape (described in Section 2.6.2), as well as its chemical composition. The canal chemistry data was assumed to be representative of the surface water across the landscape, and thus the average total P and Ca concentrations in the canals were used to determine the concentration of P and Ca found in surface water on the landscape. Mean concentration (as a normal distribution), mean water depth (a normal distribution), and depressional area provided estimates of total water P and Ca in each system.

2.6.4. Estimations of P in the periphyton compartment

We derived the areal concentration of P in periphyton from data gathered in the Long Term Ecological Research station in the Everglades (Gaiser, 2014). We assumed that periphyton grows only in the domes, as the upland matrix across much of BICY is too dry to support periphyton; as such, we estimated total periphyton P using depression area in each system.

2.7. Chemical analysis

2.7.1. Wood and rock

Caprock and wood samples were dried at 60 °C for 18 h and pulverized (rock) or finely milled (wood) in preparation for digestion. We digested the samples in nitric acid for 9 h at 138 °C and in perchloric acid for 3 h at 208 °C along with internal (KH_2PO_4) and external references (NIST-1573a and NIST-1646a) and diluted the digested samples to 75 ml with DI water according to Carter, 1993. We measured the Ca content of the rock on a Perkin Elmer 2100 atomic absorption spectrometer and the P content of the rock and wood with a Lachat QuikChem 8500 autoanalyzer for total P analysis.

2.7.2. Sediment

We measured total P content of sediment according to methods outlined in Schelske et al. (1986) by digesting 50 mg of sediment in a solution of 20 ml of 5% sulfuric acid and 10 ml of 5% potassium persulfate, which was autoclaved for 30 min. The P concentration in the solution was measured using a SEAL AA3 AutoAnalyzer. Errors on check standards and replicates were < 10%.

The calcium content of the sediment was inferred from the Total Inorganic Carbon (TIC) assuming that all carbonate in sediments is from calcite. TIC was measured using a UIC (Coulometrics) 5014 CO_2 coulometer coupled with an AutoMate automated carbonate preparation device (AutoMateFX.com). Results on the precision of the standards utilized for TIC measurements were better than 0.30 µg C per g of sample. Weight TIC percentage results from core subsections were then converted to percent Calcite and percent Ca through molar conversions.

2.7.3. Radiocarbon dating on charcoals

To provide an alternative estimate of landscape age, we sampled and radiocarbon dated charcoal samples collected from deep sediment profiles in 2 depressions. Charcoals were picked from the near bottom layers of cores taken in two domes in RP (from 101 to 104 cm in a 117 cm core and from 77 to 78 cm in an 81 cm core). Charcoals were washed in 1 N HCl at 90 °C, followed by cleaning in 0.5 N NaOH solution at 90 °C until the solution was clear. Then charcoals were washed again in 1 N HCl at 90 °C, cleaned with Milli-Q water, and dried in an oven at 60 °C.

The cleaned charcoals were transferred into quartz tubes containing CuO pellets and sealed on a vacuum line in the Organic Geochemistry Lab at the University of Florida. Charcoals were converted to CO_2 gas by combusting at 900 °C for 3 h. CO_2 gas was further purified cryogenically on the vacuum line and then sealed in Pyrex reactor tubes using the zinc reduction method (Xu et al., 2007). Purified CO_2 gas was converted to graphite by combusting at 500 °C for 3 h and subsequently at 550 °C for 4 h. Graphite samples were sent to National Ocean Sciences Accelerator Mass Specotrometry (NOSAMS) facility at the Woods Hole Oceanographic Institution for radiocarbon dating. Radiocarbon results were corrected for minor contamination in the preparation and calibrated with an IntCal 13 calibration curve.

3. Results

Our watershed size analysis indicated that the TR and RP watersheds were of similar size (TR: median 1429 km^2, 95% CI 556–5559 km^2 and RP: median 1162 km^2, 95% CI 340–6447 km^2). Uncertainty on this value is large because our method of calculating watershed size assumes no change in water storage, so any intra-annual change in groundwater, surface water, or soil moisture storage will induce variation in estimated watershed size.

The export of Ca from the landscape was remarkably chemostatic,

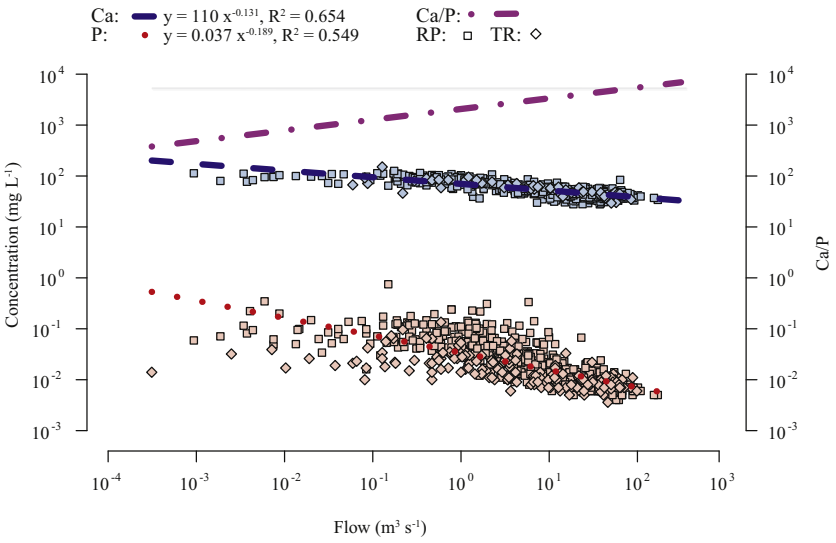

Fig. 3. Hydrologic chemical export.
Concentration/flow relationship of water flowing out of the Turner River (diamonds) and Raccoon Point (squares) watersheds. Calcium (mg Ca L^{-1}) is shown in blue and P (mg PO_4^{3-}—P L^{-1}) is shown in red. The ratio of the two elements is shown in purple and can be seen to increase at higher discharge. The grey line across the top is the Ca/P ratio of the caprock. (For interpretation of the references to colour in this figure legend, the reader is referred to the web version of this article.)

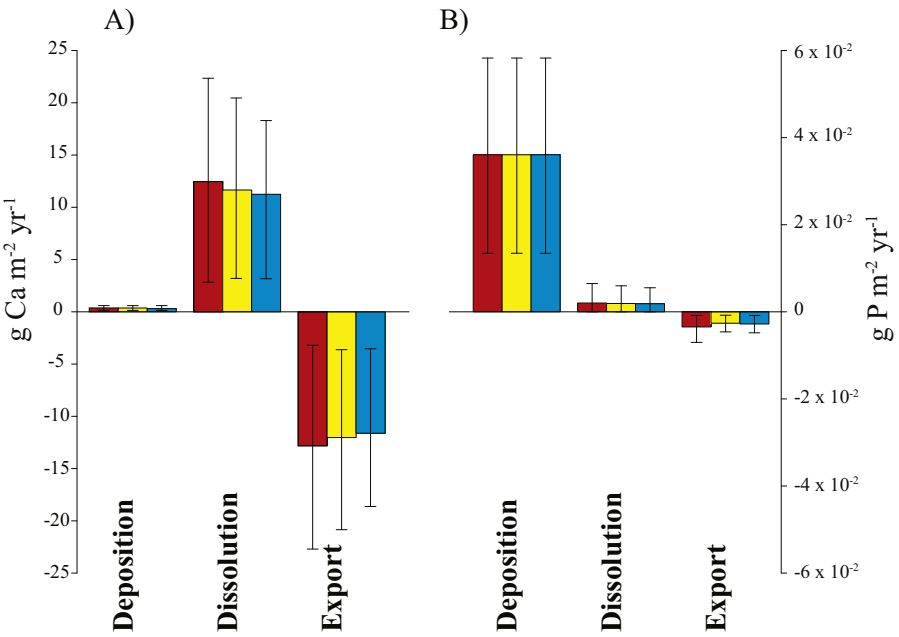

Fig. 4. Budget fluxes.
Annual aerial fluxes of A) Ca and B) P in and out of BICY. Red is RP, yellow is TR, and blue is the combination of both. The height of the bars represents the median value in the Monte Carlo, and the error bars represent the 95% confidence interval. Note that scales are different for the different elements. Ca largely flushes out of the system, while P is largely retained. Dissolution values are based on results from the Ca method. (For interpretation of the references to colour in this figure legend, the reader is referred to the web version of this article.)

with a dilution of less than an order of magnitude across 6 orders of magnitude of flow (power law slope = −0.131, Fig. 3). The concentration of P, however, was more sensitive to dilution (power law slope = −0.189). This difference in dilution rates meant that the Ca/P ratio of the exported water increased with increasing flow, approaching the Ca/P ratio of the caprock at the highest flows. Further, the concentration of P in TR canal water was lower than in RP (means 0.016 mg PO_4-P L^{-1} and 0.040 mg PO_4-P L^{-1} respectively, $t = -49.8$, df = 18,859, p < 2.2e−16), resulting in a lower mean annual mass export of P ($t = -19.2$, df = 17,720, p < 2.2e−16). The concentration of Ca also differed between the two discharge points (62.9 mg Ca L^{-1} for TR vs. 61.5 mg Ca L^{-1} for RP, $t = 6.9$, df = 35,900, p = 2.5e−12), leading to a difference in annual Ca export ($t = 11.4$, df = 16,825, p < 2.2e−16).

The Ca and P budgets were dominated by very different inputs and fates. Ca export was 60 times greater than inputs from atmospheric deposition. The inferred denudation rate via the Ca method therefore nearly matched the rate of Ca export (Fig. 4; median denudation rate 0.016 mm yr^{-1} for both RP and TR). The P budget however, showed that only about 8% of P inputs via deposition were exported in canal flow. P inputs from dissolution were negligible (< 6% of total inputs).

Though the depressions make up 26% of the landscape in both watersheds, and the watersheds are of similar sizes, the void volume of the depressions was 2 times greater in TR than in RP (median Monte Carlo values 4.2×10^8 and 2.0×10^8 m^3 respectively).

Within our system boundary (i.e., bounded at the sediment-bedrock interface), Ca was only found appreciably in the soils in the depressions. Though the concentrations were high (1–8% Ca by mass), they represent only 15% of the calcium that is estimated to have been lost based on depression volume. The soils in TR held an order of magnitude more calcium than RP, even though the TR watershed had only twice as much estimated volume loss (median Monte Carlo values 2734 g m^{-2} in RP and 48,171 g m^{-2} in TR). The calcium stored in water was negligible in comparison (medians 2.43 and 3.76 g m^{-2} in RP and TR respectively).

Similarly, the majority of P storage occurred in the soils (median Monte Carlo values 103 and 351 g m^{-2} in RP and TR respectively). In fact, the P in the soils was three orders of magnitude higher than the next largest storage pool, vegetation (median values 0.32 and 0.31 g m^{-2} in RP and TR). The water (medians 0.0014 and 0.0009 g P m^{-2} for RP and TR) and the periphyton (median value 0.003 g m^{-2} for RP and TR) were lower still. Though these areal measurements are useful for comparison between watersheds, they mask the heterogeneity of storage within each watershed. The majority of the soil, and also of the P stored in the soils, is found in the depressions themselves. Despite comprising only 26% of the landscape, roughly 6 times as much P (in g) was stored in the domes as in the upland matrix in the TR sites. This partitioning was less dramatic in RP, where P concentrations (g m^{-2}) were slightly higher in the upland than the domes, and the difference in soil depths was lower. Overall, TR held over 3 times more P on the landscape (in g m^{-2}) than RP.

The combination of observed fluxes and stocks of Ca and P suggest relatively recent formation of the BICY landscape. The oldest modal age calculated through the Monte Carlo simulation was calculated for TR through the Ca budget at 19297 years, and the youngest modal age was calculated for RP through the Joint method at 3043 years (Fig. 5). Seven of nine watershed/method combinations yielded modal ages ~10,000 years or younger. The probability mass densities of the age distributions all resembled log-normal distributions that were skewed towards younger values, and all distributions overlapped. Though the 95% confidence interval (CI) of age has a long tail, the shape of the probability density function favors values more closely constrained around the modal ages. In each watershed (TR, RP, and BICY as a whole), the P and Joint methods yielded very similar results while the Ca budget routinely predicted an older landscape. Our calculations of age based on the Ca budget did not account for the Ca stored in the sediments (found to be ~15% of the amount lost). Decreasing the ages estimated through the Ca method by 15% though would still predict an older landscape than the predictions of the P method. Age estimates of the TR landscape were consistently 2–3 times older than estimates of the RP landscape.

The estimates from the Joint and P methods are consistent with the dates derived from radiocarbon dating. The charcoal from the two cypress domes that we dated, both in RP at ~1 m depth, were 3272 ± 27 and 3311 ± 80 years which is near the modal age of the P and Joint age estimates for RP.

4. Discussion

4.1. Timescale of pattern development

Our estimated median ages range across methods (3043–19,297 years)

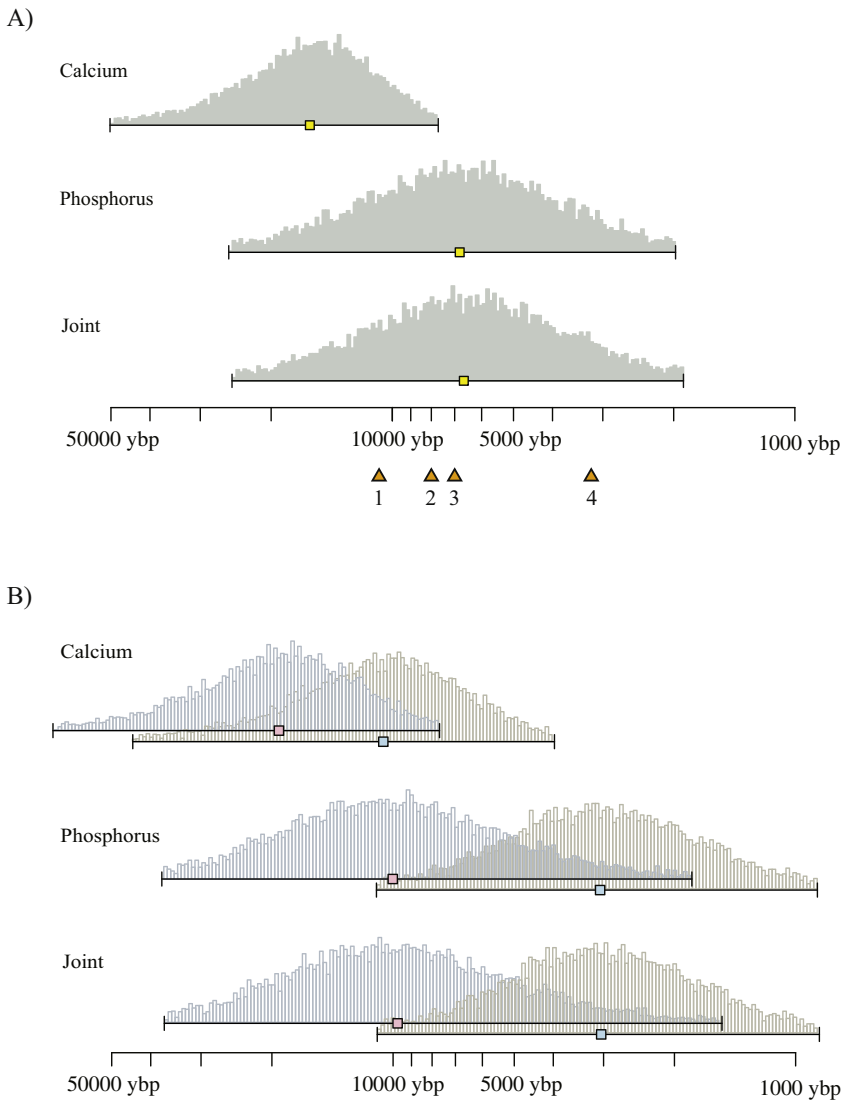

Fig. 5. Estimated ages of the big cypress patterned landscape.
Probability densities of age estimates of A) BICY and B) the RP and TR watersheds separately. TR is represented by the blue histograms, and RP is represented by the grey histograms. TR is estimated as older in all of the calculations. Each plot shows the probability density function within the 95% confidence interval, and the squares represent the mean (yellow for BICY, pink for TR and blue for RP). 1: Mechanistic age estimation of a 2 m deep depression (Dong et al., 2018) 2: Date when many of South Florida's lakes first filled in (Watts and Hansen, 1994) 3: Date when vegetation shift occurred to pine/cypress (Watts and Hansen, 1994) 4: Radiocarbon dates from RP. (For interpretation of the references to colour in this figure legend, the reader is referred to the web version of this article.)

but suggest landscape development initiation was early-mid Holocene, largely consistent with other findings and with the hypothesis of ecohydrologic feedbacks. Mechanistic modeling of BICY wetland depressions found that 2 m deep depressions would take 11,000 years to form through the hypothesized feedbacks (Dong et al., 2018). Two meters is deeper than the average depression depth in our study, perhaps representing a maximum age for the larger domes on the landscape, with smaller domes being younger. Our estimates are also in keeping with our results from the radiocarbon dating in the RP watershed, which may represent a minimum age, as charcoal could have been deposited after the depressions were formed to their current depths. Our age estimates further overlap with the paleoclimate data and pollen studies, which show a vegetation shift to cypress dominance around 5000–10,000 years ago (Watts, 1975; Watts and Hansen, 1994). In combination, the remarkable consistency of these estimates, derived from entirely independent data and assumptions, strongly indicates a Holocene origin of the Big Cypress landscape and hypotheses of its formation that operate over such timescales. To our knowledge, this paper (in conjunction with Dong et al., 2018) are the first studies to explain the timescales of development of macro-scale karst features such as those found in Big Cypress using both empirical measurements of denudation rate and theoretical estimates of weathering rate.

Alternative formation hypotheses to the ecohydrologic feedback hypothesis are that the depressions are either collapse features (sinkholes) or inherited (or partially inherited) features from some previous geological era. If these features were collapse sinkholes, our method would underestimate the void space because we would not be accounting for underground voids that have not yet collapsed. This underestimation would greatly alter the Ca budget by underestimated total Ca export and consequentially underestimating age, but would minimally impact the P budget because of the low concentration of P in the bedrock. However, considerable sampling effort to detect the sediment-bedrock interface using tile probes never revealed evidence of debris tubes or a sediment thickness > 3 m, whereas collapse features tend to generate more variable sediment thicknesses, sometimes up to 60 m in other parts of Florida (Beck, 1986). Additionally, sinkholes are generally formed via collapse in large vadose zones, and the current conditions in BICY have a high water table remaining throughout the year, which would indicate that at least in recent history sinkhole formation is unlikely (Gutierrez et al., 2014; Xiao et al., 2016). If these depressions were inherited features, we would expect less overlap between the P and Ca budgets than we observed, because the storage of P in wetland sediments would not be expected to persist during a long, dry, glaciated period, whereas cumulative exported Ca would persist between interglacial periods. Inherited features may still be a result of these same ecohydrological feedbacks, though simply knowing the age of the landscape in this case would not be able to rule out other possibilities. The chemostatic nature of Ca export (Fig. 3) indicates there may be transport limitation of dissolution in BICY. Surface discharge

limitation would also be consistent with our ecohydrologic self-organization hypothesis. We contend that these lines of evidence together support the hypothesis that these landscapes are self-organized biokarsts of relatively recent origin.

4.2. Denudation rates

Our range of calculated denudation rates (95% CI for BICY as a whole: 0.004–0.025 mm yr^{-1} through the Ca method and 0.008–0.037 mm yr^{-1} through the Joint method) are lower than many other karst denudation studies have found (Florea, 2015). Big Cypress denudation rates are only 10% of those determined in the Jura Mountains and many karst streams in the US, and they are only 1% of those determined in the Akiyoshi-dai Plateau in Japan (Akiyama et al., 2015; Calmels et al., 2014; Covington et al., 2015). Both the Jura mountains and Akiyoshi-dai Plateau have steep slopes - a condition in which mechanical erosion is likely to contribute to denudation, and in which faster flowing water will have less of a transportation barrier to dissolution (Ryb et al., 2014; Sweeting, 1973). The solubility of Ca in BICY would also be expected to be lower than areas characterized by subsurface drainage, because the contact of surface water with the atmosphere allows CO_2 to evade and therefore limits the acidity of the water. Without a continuous supply of CO_2, the concentration of carbonic acid will drop and calcium carbonate ($CaCO_3$) will precipitate. This would indicate that biological respiration may be especially important in surface water karst systems, where constant supply of organic acids and CO_2 is necessary to maintain disequilibrium with the atmosphere.

Although our budget-derived age calculations assumed constant dissolution rates, in reality dissolution rates are dependent on exposed surface area, the structure of the solution front, and local climate and vegetation community, all of which vary over time (Calmels et al., 2014; Florea, 2015; Sweeting, 1973). For example, mechanistic modeling of these dissolution processes (Dong et al., 2018) indicates that dissolution rates can increase or decrease over time as the soil layer thickens, depending on other environmental conditions. Hydrologic connectivity on the landscape also affects dissolution rates, as bedrock dissolution slows when Ca cannot be exported hydrologicaly (Cohen et al., 2011). The connectivity of wetland depressions across the landscape has likely changed over the course of landscape evolution, and may currently contribute to observed differences in denudation rates between the two watersheds.

Our estimates of both dissolution and age were based on assumptions of constant deposition and export rates. Atmospheric deposition rates have varied, and that variation would impact our P budget most strongly, as deposition is the primary source of P influx. Within the likely range of deposition variation however, our age estimates would still be Holocene. Current deposition rates are consistent with globally observed values (Redfield, 2002), though they will have varied as global wind patterns delivered more or less dust from the Sahara to Florida, and as anthropogenic disturbance increased P deposition (Mahowald et al., 2008; Mahowald et al., 2010; Prospero and Lamb, 2003). A study of cypress domes nearer to urban areas had estimates of P loading that were nearly triple those estimated in the Everglades (Brown, 1981), suggesting an upper limit of the historical expected variation. Export from the system also has likely varied over the past 10,000 years with changing connectivity and water table levels in ways that are not well understood.

One major difference between the Ca-method and the Joint method was the assumption of where dissolution occurred. Jointly solving the P and Ca budgets resulted in denudation rates higher than in solving the Ca budget alone (median Monte Carlo values 0.018 and 0.023 mm yr^{-1} for RP and TR respectively, an increase of 5–44% over the Ca method). Even so, this denudation rate over the calculated ages (48–71% younger, Fig. 5) does not achieve the observed depths of the depressions if we assume, as we did in the Ca budget, that dissolution happens only in the depressions. In RP it achieves an average depth of 21 cm as opposed to the 71 cm observed, and in TR it achieves an average depth of 83 cm as opposed to the 116 observed. However, moving from an assumption that dissolution is happening solely in the depressions and being immediately exported (Fig. 2a) to a model where some material dissolved out of the depressions is deposited on the uplands (Fig. 2c) would bring this into agreement by allowing increased dissolution rates localized in the depressions while the landscape denudation rate remains unchanged. Anecdotal evidence suggests this may occur; each year as the stage of the water recedes, it leaves behind a thin film of calcareous material. Coupled dissolution/reprecipitation systems are known to occur in streams, ocean sediments, and other karst systems (de Montety et al., 2011; Ford and Williams, 2007; Hu and Burdige, 2007).

The P-method made the assumption that P inputs from dissolution originated in the depressions, but that P was then free to move between the depressions and the uplands. Phosphorus retention on the landscape could occur both biotically and abiotically. Phosphorus is a potentially limiting element in BICY, in which case tight cycling and strong retention due to rapid biological uptake would be expected. Apatite has also been identified as an abundant mineral in several of our sediment cores. Interestingly, P retention seems to be most active at higher flows (Fig. 3), when most of the landscape is connected, and mineral sediments around the wetland depressions are inundated. The ratio of Ca/P at high flows is roughly an order of magnitude higher than at low flows, while the increase in inundated surface area is $< 3\times$. These variations with flow suggest that the uplands have a greater capacity to retain P than the wetland depressions, which would be expected if P were limiting growth in the uplands, and where carbonate minerals exposed in infrequently inundated settings have high P sorption capacity. Our study showed more P in the sediments in the wetland depressions than in the surrounding matrix, which may indicate a difference in limitation between the wetland depressions and the uplands. A previous study in BICY has also shown there to be a strong bimodality of P concentrations, with the higher concentrations in the deeper more organic soils (Watts et al., 2014). Our findings of strong P retention are consistent with literature where retention rates of up to 96% have been observed in karst (Jarvie et al., 2014).

4.3. Variation in age estimates

Though the Ca budget routinely predicted older landscapes than the P budget, an almost perfect correlation exists between age estimated from solving both jointly and the age estimated from solving the P budget ($r^2 = 0.9999$). This correlation reflects the greater flexibility in distributing stocks throughout the landscape in the P and Joint methods, as these approaches allowed any inputs from dissolution to move out of depressions and onto the uplands. It also may indicate that the P budget is better constrained than the Ca budget, with the unknown flux (inputs from dissolution) playing a less important role in the P budget than in the Ca budget. The disparity between older Ca-based and younger P-based estimates could also be explained if denudation rates were more rapid during the early evolution of this landscape. This would not affect the P-based estimates in the same way because P input from dissolution is negligible, whereas dissolution is the primary Ca input (Fig. 4).

TR and RP were characteristically different in ages across all three age estimations. This is likely due to differences in the observed denudation rates rather than actual differential dates of initiation, as denudation is likely to vary over time with sediment depth and connectivity. TR exhibits deeper depressional wetland soils (median Monte Carlo value 0.92 m vs 0.52 m in RP), and thus would be more likely to be an overestimate of the age of the landscape, and age estimates for TR are consistently older than for RP.

4.4. Mass balance approach

Mass balances of both Ca and dissolved inorganic carbon have been used to estimate denudation rates of karst landscapes (Florea, 2015; Williams and Dowling, 1979). Less common however, is an assessment of landscape age. This type of assessment requires a good estimate of the removed volume, which was possible in BICY because dissolved voids manifest as surface features, and we made use of this in our Ca budget. Florea (2015) applied mass balance denudation rates to a well-studied cave system in Kentucky, yielding estimates in agreement with other regional measurements, suggesting that this approach is broadly applicable where void space can be determined. Our P and Joint budgets were also developed as independent estimates on this unique landscape. These budgets did not require knowing the void space, but rather considered standing stocks on a landscape of time-variable depth when constructing the budget.

The probability distributions of age were skewed young, but had long tails resembling log-normal distributions as would be expected statistically through the multiplication of independent variables. The uncertainty in ages arises mostly from uncertainty in fluxes rather than uncertainty in stocks. Though scaling from point measurements to landscape stocks incorporates many assumptions about the representativeness of sampling, the spatial heterogeneity of fluxes (especially atmospheric deposition and dissolution) are equally as uncertain. Increasing the number of habitat types on the landscape allowed us to better account for spatial heterogeneity in our calculations. Uncertainty in fluxes is amplified by the thousands of years for which we have no direct measurements. Our ability to account for temporal variability was limited to the 50 years of hydrologic export data. This allowed us to incorporate modern inter-annual variation, but its ability to estimate an entire geological epoch was understandably limited. We used a Monte Carlo simulation to more simply allow uncertainty to propagate forward from each of the many parameters included. Traditional propagation of error was less informative, especially when solving the budgets jointly, which required matrix algebra to solve, as not all parameters were normally distributed.

Even with all this uncertainty, we were able to see that the age of this landscape coincides with the same general timeframe as major vegetation and climate change (independent estimates of which also contain uncertainty) as well as with radiocarbon and mechanistic modeling estimates of basin initiation. It is clear that mass balance is most informative when combined with other methods of age estimation and when including multiple elements, but the consonance of estimates indicates the utility of our simple method.

4.5. Biogeomorphic niche construction

Ecologically, the process of species altering their environment in ways that advantage them is well established (Phillips, 2016b; Stallins, 2006). Though our analysis does not distinguish between climatic and biological effects on dissolution, high rates of CO_2 production by respiration imply that the wetland ecosystems are contributing to dissolution through acidification of soil porewater. Numerical models parameterized for the climatic condition of BICY suggested that without CO_2 provided by plant root respiration, the maximum amount of dissolution in the past 10 kyrs is about 0.1 m (Dong et al., 2018). A study across cypress domes and scrub cypress (the same landscape as our dwarf cypress matrix) found that soil respiration in the scrub cypress was less than half that of domes, which would have an important influence on dissolution rates under the two habitats (Brown, 1981). At the very least this would suggest that active ecosystem engineering is taking place. If cypress trees, or other wetland plant species, are benefiting competitively by this contribution to dissolution, which they seem to based on their distribution, this could form a local positive feedback, which when coupled with a distal negative feedback (such as limitation of water) may explain the apparent regular patterns in the landscape (Watts et al., 2014). Such a competitive advantage would be considered active niche construction by the cypress trees (Phillips, 2016b). Previous studies of carbonate systems have indicated that the form of the vegetative community has impacts on rates of dissolution (Calmels et al., 2014; Zhang, 2011 but see Plan, 2005 who found only the presence of vegetation to be important and not the community composition). However, mechanisms leading past biogeomorphic effects into the realm of niche construction have not yet been established in any systems.

5. Conclusion

We used two elemental budgets to determine relatively recent (Holocene) ages of depressional wetlands in the karst landscape of BICY. This age is consistent with other age estimates of the landscape, and is consistent with an ecohydrologic and geochemical feedback hypothesis of karst depression formation. Our work highlights the value of explicitly considering uncertainty in mass balance studies, especially when linking mass fluxes to timescales of landscape evolution, and shows the utility of this simple approach to age estimation. Though biokarst is seldom considered above the microscale (Cunningham et al., 1995; Duane et al., 2003; Fiol et al., 1996; Viles, 1984, but see de la Rosa, 2016 who considered biokarst at the *meso*-scale), this study indicates that meso and macro scale karst formations may also be attributable to biokarst processes. This implies that future karst evolution studies at this scale should actively consider the role of biota in their analyses.

Acknowledgements

We would like to thank C. Clifford for help with fieldwork, and B. Hassett, P. Heine and W. Cook for assistance with the chemical analysis. E. Bernhardt and R. Marinos provided comments on an early draft, and A. Braswell, M. Fork, C. Clifford and J. Gardner have provided valuable feedback at many steps. We would also like to thank our two anonymous reviewers for their helpful comments and suggestions. Samples for this work were collected under NPS permit #BICY-2016-SCI-0008.

Funding sources

Funding came from the National Science Foundation through award DEB#1354783, and through a Graduate Research Fellowship Program award to C. Chamberlin. The NSF had no involvement in the conduct of this research or in the preparation of the article.

Competing interests

No conflicts of interest.

References

Ahn, H., James, R.T., 2001. Variability, uncertainty, and sensitivity of phosphorus deposition load estimates in South Florida. Water Air Soil Pollut. 126 (1–2), 37–51.

Akiyama, S., Hattanji, T., Matsushi, Y., Matsukura, Y., 2015. Dissolution rates of subsoil limestone in a doline on the Akiyoshi-dai Plateau, Japan: an approach from a weathering experiment, hydrological observations, and electrical resistivity tomography. Geomorphology 247, 2–9.

Beck, B.F., 1986. A generalized genetic framework for the development of sinkholes and karst in Florida, USA. Environ. Geol. Water Sci. 8 (1–2), 5–18.

Bormann, F.H., Likens, G.E., 1967. Nutrient cycling. Science 155 (3761), 424–429.

Brown, S., 1981. A comparison of the structure, primary productivity, and transpiration of cypress ecosystems in Florida. Ecol. Monogr. 51 (4), 403–427.

Calmels, D., Gaillardet, J., Francois, L., 2014. Sensitivity of carbonate weathering to soil CO2 production by biological activity along a temperate climate transect. Chem. Geol. 390, 74–86.

Camazine, S., 2001. Self-organization in Biological Systems. Princeton Studies in Complexity. Princeton University Press, Princeton, N.J. (viii, 538 p., 8 p. of plates pp).

Carter, M.R., 1993. Soil Sampling and Methods of Analysis. Lewis Publishers, Boca Raton (823 pp.).

Chojnacky, D.C., Heath, L.S., Jenkins, J.C., 2014. Updated generalized biomass equations for North American tree species. Forestry 87 (1), 129–151.
Cohen, M.J., Watts, D.L., Heffernan, J.B., Osborne, T.Z., 2011. Reciprocal biotic control on hydrology, nutrient gradients, and landform in the greater everglades. Crit. Rev. Environ. Sci. Technol. 41 (sup1), 395–429.
Coleborn, K., et al., 2016. Effects of wildfire on long-term soil CO2 concentration: implications for karst processes. Environ. Earth Sci. 75 (4).
Covington, M.D., Gulley, J.D., Gabrovsek, F., 2015. Natural variations in calcite dissolution rates in streams: controls, implications, and open questions. Geophys. Res. Lett. 42 (8), 2836–2843.
Cunningham, K.I., Northup, D.E., Pollastro, R.M., Wright, W.G., Larock, E.J., 1995. Bacteria, fungi and biokarst in Lechuguilla Cave, Carlsbad-Caverns-National-Park, New-Mexico. Environ. Geol. 25 (1), 2–8.
Davis, S.M., Ogden, J.C., 1994. Everglades: the ecosystem and its restoration. In: Everglades: The Ecosystem and Its Restoration: i–xv, pp. 1–826.
Doctor, D.H., Young, J.A., 2013. An Evaluation of Automated GIS Tools for Delineating Karst Sinkholes and Closed Depressions from 1-Meter Lidar-Derived Digital Elevation Data. In: Land, L., Doctor, D.H., Stephenson, J.B. (Eds.), 13th Multidisciplinary Conference on Sinkholes and the Engineering and Environmental Impacts of Karst. National Cave and Karst Research Institute, Carlsbad, New Mexico.
Dong, X., Cohen, M.J., Martin, J.B., McLaughlin, D.L., Murray, A.B., Ward, N.D., Flint, M.K., Heffernan, J.B., 2018. Ecohydrologic processes and soil thickness feedbacks control limestone-weathering rates in a karst landscape. Chem. Geol. http://dx.doi.org/10.1016/j.chemgeo.2018.05.021.
Duane, M.J., Al-Mishwat, A.T., Rafique, M., 2003. Weathering and biokarst development on marine terraces, northwest Morocco. Earth Surf. Process. Landf. 28 (13), 1439–1449.
Dubois, C., et al., 2014. The process of ghost-rock karstification and its role in the formation of cave systems. Earth Sci. Rev. 131, 116–148.
Ewel, K.C., Wickenheiser, L.P., 1988. Effect of swamp size on growth-rates of cypress (Taxodium-distichum) trees. Am. Midl. Nat. 120 (2), 362–370.
Fiol, L., Fornos, J.J., Gines, A., 1996. Effects of biokarstic processes on the development of solutional Rillenkarren in limestone rocks. Earth Surf. Process. Landf. 21 (5), 447–452.
Florea, L.J., 2015. Carbon flux and landscape evolution in epigenic karst aquifers modeled from geochemical mass balance. Earth Surf. Process. Landf. 40 (8), 1072–1087.
Folk, R.L., Roberts, H.H., Moore, C.H., 1973. Black phytokarst from Hell, Cayman-Islands, British-West-Indies. Geol. Soc. Am. Bull. 84 (7), 2351–2360.
Ford, D., Williams, P.W., 2007. Karst Hydrogeology and Geomorphology. John Wiley & Sons, Chichester, England; a Hoboken, NJ (ix, 562 pp.).
Gaiser, E., 2014. In: Network, L.T.E.R. (Ed.), Periphyton Biomass Accumulation from the Shark River and Taylor Sloughs, Everglades National Park (FCE), from January 2003 to Present.
Gutierrez, F., Parise, M., De Waele, J., Jourde, H., 2014. A review on natural and human-induced geohazards and impacts in karst. Earth Sci. Rev. 138, 61–88.
Hu, X.P., Burdige, D.J., 2007. Enriched stable carbon isotopes in the pore waters of carbonate sediments dominated by seagrasses: evidence for coupled carbonate dissolution and reprecipitation. Geochim. Cosmochim. Acta 71 (1), 129–144.
Jarvie, H.P., et al., 2014. Phosphorus retention and remobilization along hydrological pathways in karst terrain. Environ. Sci. Technol. 48 (9), 4860–4868.
Khadka, M.B., Martin, J.B., Jin, J., 2014. Transport of dissolved carbon and CO2 degassing from a river system in a mixed silicate and carbonate catchment. J. Hydrol. 513, 391–402.
de la Rosa, J.P.M., 2016. The Burren: a glacial, karstic and biokarstic expression of a limestone plateau in western Ireland. Earth Surf. Process. Landf. 41 (11), 1614–1628.
Liu, Z.H., Li, Q., Sun, H.L., Wang, J.L., 2007. Seasonal, diurnal and storm-scale hydrochemical variations of typical epikarst springs in subtropical karst areas of SW China: soil CO2 and dilution effects. J. Hydrol. 337 (1–2), 207–223.
Mahowald, N., et al., 2008. Global distribution of atmospheric phosphorus sources, concentrations and deposition rates, and anthropogenic impacts. Glob. Biogeochem. Cycles 22 (4).
Mahowald, N.M., et al., 2010. Observed 20th century desert dust variability: impact on climate and biogeochemistry. Atmos. Chem. Phys. 10 (22), 10875–10893.
Martin, J.B., 2017. Carbonate minerals in the global carbon cycle. Chem. Geol. 449, 58–72.
Mcpherson, B.F., 1974. The big cypress swamp. In: Society, M.G. (Ed.), Environments of South Florida: Present and Past, Miami, Florida.
Mitchell, K., 2015. Quantitative Analysis by the Point-Centered Quarter Method. http://peaople.hws.edu/mitchell/PCQM.pdf.
Mitchell-Tapping, H.J., Lee, T.J., Mitchell-Tapping, A.M., 1996. Core Evidence for a Major Marine Transgression During the Holocene of Southwestern Florida. Transactions of the Gulf Coast Association of Geological Societies. 46.
Monk, C.D., Brown, T.W., 1965. Ecological consideration of cypress heads in northcentral Florida. Am. Midl. Nat. 74 (1), 126.
de Montety, V., Martin, J.B., Cohen, M.J., Foster, C., Kurz, M.J., 2011. Influence of diel biogeochemical cycles on carbonate equilibrium in a karst river. Chem. Geol. 283 (1–2), 31–43.
Parkinson, R.W., 1989. Decelerating Holocene Sea-level rise and its influence on Southwest Florida coastal evolution - a transgressive regressive stratigraphy. J. Sediment. Petrol. 59 (6), 960–972.
Perne, M., Covington, M., Gabrovsek, F., 2014. Evolution of karst conduit networks in transition from pressurized flow to free-surface flow. Hydrol. Earth Syst. Sci. 18 (11), 4617–4633.
Phillips, J.D., 2016a. Biogeomorphology and contingent ecosystem engineering in karst landscapes. Prog. Phys. Geogr. 40 (4), 503–526.
Phillips, J.D., 2016b. Landforms as extended composite phenotypes. Earth Surf. Process. Landf. 41 (1), 16–26.
Plan, L., 2005. Factors controlling carbonate dissolution rates quantified in a field test in the Austrian alps. Geomorphology 68 (3–4), 201–212.
Plummer, L.N., Wigley, T.M.L., 1976. Dissolution of calcite in Co2-saturated solutions at 25 °C and 1 atmosphere total pressure. Geochim. Cosmochim. Acta 40 (2), 191–202.
Plummer, L.N., Wigley, T.M.L., Parkhurst, D.L., 1978. The kinetics of calcite dissolution in CO 2 -water systems at 5 degrees to 60 degrees C and 0.0 to 1.0 atm CO 2. Am. J. Sci. 278 (2), 179–216.
Prospero, J.M., Lamb, P.J., 2003. African droughts and dust transport to the Caribbean: climate change implications. Science 302 (5647), 1024–1027.
Redfield, G.W., 2002. Atmospheric deposition of phosphorus to the everglades: concepts, constraints, and published deposition rates for ecosystem management. ScientificWorldJournal 2, 1843–1873.
Rietkerk, M., van de Koppel, J., 2008. Regular pattern formation in real ecosystems. Trends Ecol. Evol. 23 (3), 169–175.
Ryb, U., et al., 2014. Styles and rates of long-term denudation in carbonate terrains under a Mediterranean to hyper-arid climatic gradient. Earth Planet. Sci. Lett. 406, 142–152.
Schelske, C.L., Conley, D.J., Stoermer, E.F., Newberry, T.L., Campbell, C.D., 1986. Biogenic silica and phosphorus accumulation in sediments as indexes of eutrophication in the Laurentian Great-Lakes. Hydrobiologia 143, 79–86.
Shoemaker, W.B., Lopez, C.D., Duever, M.J., 2011. In: USGS (Ed.), Evapotranspiration over Spatially Extensive Plant Communities in the Big Cypress National Preserve, Southern Florida, 2007–2010: Scientific Investigations Report 2011–5212, pp. 46.
Solomon, D.K., Cerling, T.E., 1987. The annual carbon-dioxide cycle in a montane soil - observations, modeling, and implications for weathering. Water Resour. Res. 23 (12), 2257–2265.
Stallins, J.A., 2006. Geomorphology and ecology: unifying themes for complex systems in biogeomorphology. Geomorphology 77 (3–4), 207–216.
Sterner, R.W., Elser, J.J., 2002. Ecological Stoichiometry: The Biology of Elements from Molecules to the Biosphere. Princeton University Press, Princeton (xxi, 439 pp.).
Sullivan, P.L., et al., 2016. Trees: a powerful geomorphic agent governing the landscape evolution of a subtropical wetland. Biogeochemistry 128 (3), 369–384.
Sweeting, M.M., 1973. Karst Landforms. Columbia University Press, New York (xvi, 362 pp.).
Thornberry-Ehrlich, T., 2008. Big Cypress National Preserve Geologic Resource Evaluation Report, National Resource Report NPS/NRPC/GRD/NRR - 2008/021. National Park Service, Denver, Colorado.
Toscano, M.A., Macintyre, I.G., 2003. Corrected western Atlantic sea-level curve for the last 11,000 years based on calibrated C-14 dates from Acropora palmata framework and intertidal mangrove peat. Coral Reefs 22 (3), 257–270.
Viles, H.A., 1984. Biokarst - review and prospect. Prog. Phys. Geogr. 8 (4), 523–542.
Watts, W.A., 1975. Late quaternary record of vegetation from Lake Annie, south-Central Florida. Geology 3 (6), 344–346.
Watts, W.A., Hansen, B.C., 1994. Pre-Holocene and Holocene pollen records of vegetation history from the Florida Peninsula and their climatic implications. Palaeogeogr. Palaeoclimatol. Palaeoecol. 109 (2–4), 163–176.
Watts, A.C., Kobziar, L.N., Snyder, J.R., 2012. Fire reinforces structure of Pondcypress (*Taxodium distichum* var. imbricarium) domes in a wetland landscape. Wetlands 32 (3), 439–448.
Watts, A.C., et al., 2014. Evidence of biogeomorphic patterning in a low-relief karst landscape. Earth Surf. Process. Landf. 39 (15), 2027–2037.
Williams, P.W., Dowling, R.K., 1979. Solution of marble in the karst of the pikikiruna range, northwest Nelson, New-Zealand. Earth Surf. Process. Landf. 4 (1), 15–36.
Xiao, H., Kim, Y.J., Nam, B.H., Wang, D.B., 2016. Investigation of the impacts of local-scale hydrogeologic conditions on sinkhole occurrence in East-Central Florida, USA. Environ. Earth Sci. 75 (18), 16.
Xu, X., et al., 2007. Modifying a sealed tube zinc reduction method for preparation of AMS graphite targets: reducing background and attaining high precision. Nucl. Instrum. Methods Phys. Res., Sect. B 259 (1), 320–329.
Yang, H., Zhou, L., Huang, L.Y., Cao, J.H., Groves, C., 2015. A comparative study of soil carbon transfer between forest soils in subtropical karst and clasolite areas and the karst carbon sink effect in Guilin, Guangxi, China. Environ. Earth Sci. 74 (2), 921–928.
Zhang, C., 2011. Carbonate rock dissolution rates in different landuses and their carbon sink effect. Chin. Sci. Bull. 56 (35), 3759–3765.
Zhao, M., Zeng, C., Liu, Z.H., Wang, S.J., 2010. Effect of different land use/land cover on karst hydrogeochemistry: a paired catchment study of Chenqi and Dengzhanhe, Puding, Guizhou, SW China. J. Hydrol. 388 (1–2), 121–130.